Monthly Notices of the ROYAL ASTRONOMICAL SOCIETY

Mon. Not. R. Astron. Soc. **426,** 3490–3500 (2012) doi:10.1111/j.1365-2966.2012.22025.x

A deep, wide-field study of Holmberg II with Suprime-Cam: evidence for ram pressure stripping⋆

Edouard J. Bernard,[1†] Annette M. N. Ferguson,[1] Michael K. Barker,[1] Michael J. Irwin,[2] Pascale Jablonka[3,4] and Nobuo Arimoto[5,6]

[1]*SUPA, Institute for Astronomy, University of Edinburgh, Royal Observatory, Blackford Hill, Edinburgh EH9 3HJ*
[2]*Institute of Astronomy, Cambridge University, Cambridge CB3 0HA*
[3]*Laboratoire d'Astrophysique, Ecole Polytechnique Fédérale de Lausanne (EPFL), Observatoire, CH-1290 Sauverny, Switzerland*
[4]*GEPI, Observatoire de Paris, CNRS UMR 8111, Université Paris Diderot, F-92125 Meudon Cedex, France*
[5]*Subaru Telescope, 650 North A'ohoku Place, Hilo, HI 96720, USA*
[6]*Graduate University for Advanced Studies, 2-21-1 Osawa, Mitaka, Tokyo 181-8588, Japan*

Accepted 2012 August 31. Received 2012 August 23; in original form 2012 July 25

ABSTRACT

We present a deep, wide-field optical study of the M81 group dwarf galaxy Holmberg II (HoII) based on Subaru/Suprime-Cam imaging. Individual stars are resolved down to $I \sim 25.2$, that is, about 1.5 mag below the tip of the red giant branch (RGB). We use resolved star counts in the outskirts of the galaxy to measure the radial surface brightness profile down to $\mu_V \sim 32$ mag arcsec^{-2}, from which we determine a projected exponential scalelength of 0.70 ± 0.01 arcmin (i.e. 0.69 ± 0.01 kpc). The composite profile, ranging from the cored centre out to $R = 7$ arcmin, is best fitted by an Elson–Fall–Freeman profile which gives a half-light radius of 1.41 ± 0.04 arcmin (i.e. 1.39 ± 0.04 kpc), and an absolute magnitude $M_V = -16.3$. The low surface brightness stellar component of HoII is regular and symmetric and has an extent much smaller than the vast H I cloud in which it is embedded. We compare the spatial distribution of the young, intermediate-age and old stellar populations, and find that the old RGB stars are significantly more centrally concentrated than the young stellar populations, contrary to what is observed in most dwarf galaxies of the local Universe. We discuss these properties in the context of the comet-like distribution of H I gas around HoII, and argue for the presence of a hot intragroup medium in the vicinity of HoII to explain the contrasting morphologies of gas and stars.

Key words: galaxies: dwarf – galaxies: groups: individual: M81 group – galaxies: individual: Holmberg II – intergalactic medium – galaxies: irregular – galaxies: stellar content.

1 INTRODUCTION

In spite of their intrinsic faintness and minimal contribution to the total light, the stellar outskirts of galaxies hold crucial information about the processes of galaxy formation and evolution. Interactions, mergers and accretions all leave their imprint on the outer stellar populations in the form of substructures, streams and diffuse haloes. In addition, the long evolutionary time-scales and high sensitivity to external influences mean that coherent substructures are easier to detect and longer lived than in the denser inner regions.

Considerable effort has been devoted to studying the outer regions of massive galaxies (see e.g. Barker et al. 2012, and references therein) which, according to hierarchical models of galaxy formation, have acquired a significant fraction of their mass through mergers and accretion episodes. The stellar peripheries of low-mass dwarf galaxies have been much less studied. Most work to date has focused on Local Group galaxies (e.g. Fornax: Coleman et al. 2005; NGC 6822: de Blok & Walter 2006; Sculptor: Westfall et al. 2006), although a few dwarfs in nearby groups have also been targeted (e.g. Ryś et al. 2011). The strong morphology–density relation exhibited by dwarf galaxies suggests external mechanisms play a major role in shaping their evolution (e.g. Weisz et al. 2011); surveying their stellar outskirts may therefore yield clues on the dominant processes involved.

The global picture emerging from previous work is that most dwarf galaxies have a smooth, and generally old and metal-poor

⋆ Based on data collected at the Subaru Telescope, which is operated by the National Astronomical Observatory of Japan.

†E-mail: ejb@roe.ac.uk

'halo' surrounding a more concentrated, younger and/or more metal-rich population. While the stellar haloes of large galaxies are believed to have formed from the accretion of smaller galaxies at high redshift, it is unclear whether this process has been significant in dwarfs. For example, pure accretion cannot explain the main properties of dwarf galaxies' haloes, that is, smooth distribution, and the existence of age and/or metallicity gradients. Instead, these observations suggest either a 'shrinking' scenario, in which the region of active star formation contracts as gas supply diminishes (Hidalgo et al. 2009; Zhang et al. 2012) or radial migration of stars formed close to the centre towards the outskirts (Stinson et al. 2009).

Here we analyse the stellar outskirts of the dwarf galaxy Holmberg II (hereafter abbreviated as HoII). HoII is a dwarf irregular galaxy in the M81 group that was discovered by Holmberg (1950) while surveying the galaxies in this group. Due to its location on the near-side of the group [$(m - M)_0 = 27.65$ i.e. 3.4 Mpc], as well as its proximity to the Sc spiral galaxy NGC 2403 and similar radial velocity, it is usually associated with the NGC 2403 subgroup along with three other dwarf irregular galaxies (Karachentsev et al. 2002). HoII is very similar to the Small Magellanic Cloud (SMC) in terms of absolute magnitude, H I and total mass: $M_B \sim -16.7$, $M_{\rm H\,I} \sim 6 \times 10^8\,{\rm M}_\odot$ and $M_{\rm tot} = 2.1 \times 10^9\,{\rm M}_\odot$ (Walter et al. 2007; Oh et al. 2011) compared to $M_B \sim -16.1$, $M_{\rm H\,I} \sim 4 \times 10^8\,{\rm M}_\odot$ and $M_{\rm tot} = 2.4 \times 10^9\,{\rm M}_\odot$ for the SMC (Stanimirovic et al. 1999; Stanimirović, Staveley-Smith & Jones 2004).

While HoII has been observed at all wavelengths, to date the only deep resolved stellar population study comes from *HST*/ACS observations (Weisz et al. 2009) which cover a relatively small fraction of the galaxy. The need for deep wider data is especially motivated by the striking morphology of its H I cloud. From deep Very Large Array data, Bureau & Carignan (2002, hereafter BC02) found that the distribution of neutral hydrogen has a cometary appearance – compressed on one side with a faint extended component on the opposite side – with the tail pointing away from the centre of the M81 group. BC02 argued that HoII is moving towards the M81 group and that ram pressure from a hot intragroup medium (IGM) is responsible for the H I morphology, although they could not rule out the alternative interpretation of a gravitational interaction between HoII and one of its fainter neighbours.

Possible signatures of ram pressure stripping have been observed in a number of galaxies of the local universe (e.g. Condon 1983; Gavazzi et al. 1995; Ryder et al. 1997; Kenney, van Gorkom & Vollmer 2004; Chung et al. 2007; McConnachie et al. 2007). However, most of these galaxies are too distant to be resolved into individual stars and their analyses have been confined to fairly high surface brightness inner regions. Knowledge of the distribution of resolved stellar populations at very large radii is fundamental because the stars do not respond to ram pressure. On the other hand, tidal forces affect gas and stars equally so both components should exhibit similar asymmetries. Comparing the large-scale distribution of the stars to that of the gas in HoII has the potential to reveal whether the H I morphology was caused by ram pressure, tidal forces, or a combination of both.

In this paper, we present a deep, wide-field study of HoII based on Subaru/SuprimeCam data, and analyse the properties of its stellar populations in the context of the comet-like shape of the H I cloud in which it is embedded. In Section 2, we describe the observations and data reduction, and present the resulting colour–magnitude diagrams (CMDs) in Section 3. The spatial distribution of the various stellar populations is described in Section 4. In Section 5, we present the radial profile and constrain the spatial extent of HoII. We discuss the implications of our results regarding the peculiar stellar and H I distributions in Section 6, and summarize the main results in Section 7.

2 OBSERVATIONS AND DATA REDUCTION

2.1 Observations and image processing

The observations of HoII (=UGC 4305 =DDO 50 =Arp 268) were obtained in service mode with the Suprime-Cam instrument (Miyazaki et al. 2002) on the 8-m Subaru telescope (PI.: M. Barker). The data were acquired on the night of 2009 December 18. Suprime-Cam is a mosaic camera made of 10 chips disposed in two rows of five chips – thus producing 10 images per exposure – leading to a large field of view (FOV; $34 \times 27\,{\rm arcmin}^2$). A single pointing was therefore sufficient to cover the relatively small galaxy ($R_{25} = 4.1$ arcmin; from HyperLeda: Paturel et al. 2003), including the large H I cloud in which it is embedded ($R \sim 16$ arcmin; BC02). This is illustrated in Fig. 1, showing the *V*-band mosaic from our Subaru data where the H I contours from BC02 have been overlaid.

10 exposures were obtained in each band, with individual exposure times of 600 s in Johnson *V* and 240 s in Cousin *I*. A small dithering pattern was used to cover the gaps between the chips as well as limit the effects of bad pixels and other camera defects, resulting in a mosaic image of $\sim 35.8 \times 29.3\,{\rm arcmin}^2$. The observations were carried out in photometric conditions, with the seeing in the range 0.65–0.95 arcsec. However, due to HoII's location at high declination, it can only be observed at relatively large airmasses from Hawaii ($\gtrsim 1.6$), so the median seeing measured in the *V* and *I* images is 0.96 and 0.76 arcsec, respectively.

The image processing procedures were similar to those followed by Barker et al. (2009, 2012). After converting each exposure to a single multiextension FITS file, all images and calibration frames were run through a variant of the data reduction pipeline developed for processing Wide Field Camera (WFC) data from the Isaac Newton Telescope (INT) (for further details see Irwin 1985, 1997; Irwin & Lewis 2001; Irwin et al. 2004).

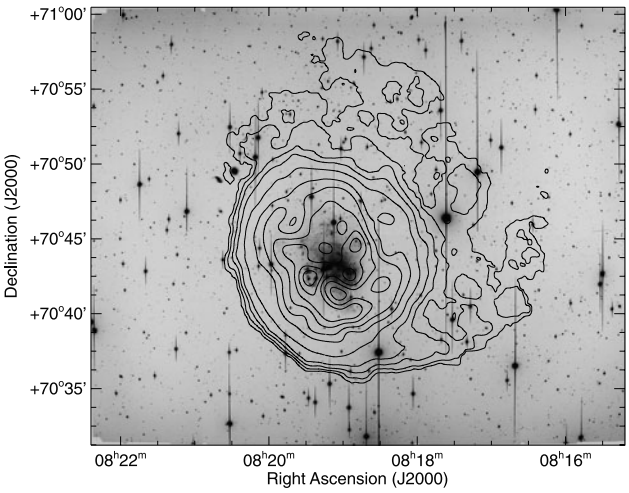

Figure 1. Mosaic *V* image of HoII, showing the whole FOV of our Subaru data ($\sim 35.8 \times 29.3\,{\rm arcmin}^2$). The H I contours from BC02, ranging from $N_{\rm H\,I} = 0.1$ to 19×10^{20} atoms cm^{-2}, are overplotted. Note the comet-like morphology of the outermost contour.

First-stage image processing steps included bias and overscan correction, together with trimming to the reliable active detector area. Master flats were created by stacking a dithered set of 10 *V* and 12 *I* twilight sky exposures. The flat-fielding step also corrects for internal gain variations between the detectors. After flat-fielding the dark sky *I*-band images were examined for signs of fringing, but as for other similar Subaru data, this was found to be negligible.

Prior to stacking, detector-level catalogues were generated for each individual processed science image to refine the astrometric calibration and also to assess the data quality. For astrometric calibration, a Zenithal polynomial projection (Greisen & Calabretta 2002) was used to define the World Coordinate System (WCS). A fifth-order polynomial includes all the significant telescope radial field distortions leaving just a six-parameter linear model per detector to completely define the required astrometric transformations. The Two-Micron All-Sky Survey point-source catalogue (Cutri et al. 2003) was used for the astrometric reference system.

During the stacking process, the individual Subaru catalogues were used in addition to the standard WCS solution, to further refine to the subpixel level the alignment of the component images. The common background regions in the overlap area from each image in the stack were used to compensate for sky variations during the exposure sequence and the final stack included seeing weighting, confidence (i.e. variance) map weighting and clipping of cosmic rays.

As a final image processing step, catalogues were derived from the deep stacks for each detector and their WCS astrometry was updated prior to forming the mosaic over all detectors. Any residual small offsets in the underlying sky level between detector stacks were removed iteratively by visual inspection of a 4×4 blocked mosaic of the whole field.

Full-resolution mosaics were used to provide an initial set of full-field catalogues based on standard aperture photometry (e.g. Irwin et al. 2004). Since no standard star field was observed, we used INT WFC *V*- and *i*-band observations centred on HoII and taken in photometric conditions during 2009 April to derive the photometric calibration for the mosaics. The INT WFC *V*,*i* photometry was first converted to the Johnson–Cousins system (e.g. McConnachie et al. 2003) and then directly used to calibrate the Subaru data with an estimated systematic error of ± 2 per cent.

Fig. 2 shows a colour composite image obtained from the *V* and *I* mosaics, which highlights the irregular morphology and strong contribution from the young, blue supergiant stars.

2.2 Profile-fitting photometry

Given the very high stellar density in HoII, we subsequently decided to perform profile-fitting photometry which is better suited to obtain accurate measurements in crowded fields. The point spread function (PSF) photometry was carried out with the DAOPHOT/ALLSTAR/ALLFRAME suite of programs (Stetson 1994) as follows. We performed a first source detection at the 3σ level on the individual images, which was used as input for aperture photometry. From these catalogues, 300 bright, non-saturated stars per image were initially selected as potential PSF stars. An automatic rejection based on the shape parameters was used to clean the lists, followed by a visual inspection of all the stars to remove the remaining unreliable stars. We ended up with clean lists containing at least 150 good PSF stars per image. Modelling of the empirical PSF with a radius of 12 pixels was done iteratively with DAOPHOT: the clean lists were used to remove all the stars from the images except PSF stars, so that accurate PSFs could be created from non-crowded stars. At each iteration, the PSF was modelled more accurately and thus the neighbouring stars removed better. Every three to five iterations, the degree of PSF variability across the image was also increased, from constant to linear, then quadratically variable.

The following step consisted of profile-fitting photometry on the individual images using ALLSTAR with the empirical PSFs previously created. The resulting catalogues were matched on a chip-by-chip basis, keeping only the objects for which the PSF fitting converged in at least three images per band to limit the number of false detections, to create one clean stellar catalogue per chip. These catalogues were further cleaned by rejecting extended objects based on the sharpness parameter, then merged to produce a master catalogue for the whole Suprime-Cam FOV. This catalogue was then used as the input star list for ALLFRAME, which was run on all the individual images at once. The output of ALLFRAME consists of a catalogue of PSF photometry for each individual image. A robust mean magnitude was obtained for each star by matching these catalogues.

The final photometry was calibrated to the Johnson–Cousin standard system by matching $\sim$1750 bright stars in common with the calibrated aperture photometry described in the previous section. The uncertainty on the offset between the aperture and PSF photometry is smaller than 0.001 in both bands and therefore represents a negligible contribution to the total magnitude uncertainties.

According to the Schlegel, Finkbeiner & Davis (1998) reddening maps, the area covered by our observations suffers from minor foreground differential reddening, with $E(B-V)$ ranging from about 0.023 to 0.033. To obtain accurate photometry over the whole FOV, each individual star was corrected for reddening based on its location. We note that the corresponding dust mask map indicates that a small area centred on HoII (out to $r \sim 6$ arcmin; i.e. $\sim$10 per cent of the Subaru FOV), as an extragalactic source, was removed from the dust map and replaced with the median value of the surrounding pixels. This means that the star-by-star correction does not include extinction internal to HoII.

Finally, the astrometric calibration for the whole stellar catalogue was obtained with the IRAF tasks *ccxymatch*, *ccmap* and *cctran* using $\sim$800 stars in common with Version 2.3.2 of the Guide Star Catalog II (Lasker et al. 2008). The accuracy of the resulting astrometry is about 0.3 arcsec.

2.3 Completeness

To estimate the completeness of our data, we retrieved the *HST*/ACS photometry of HoII from the ACS Nearby Galaxy Survey Treasury programme (Dalcanton et al. 2009). While it only covers a tiny fraction of our FOV ($\sim$2 per cent), it is located on the highest density area which is the most affected by incompleteness. It is $\sim$3 mag deeper than our Subaru photometry and much less affected by stellar crowding, thanks to the higher spatial resolution of the instrument. Therefore, in the following we assume that it is 100 per cent complete in the range of magnitudes covered by our Subaru data, and representative of the intrinsic photometric properties of the stars in HoII.

We used DAOMATCH and DAOMASTER (Stetson 1993) to match the *HST* and Subaru photometric catalogues. These programs are based on the robust 'matching triangles' technique, rather than assuming a given matching radius. This ensures a proper matching of the stars even in very crowded regions, regardless of the possible translations, rotations, scale changes or flips of the coordinate systems.

Using all the stars from the area in common between the two photometric catalogues, we find the 50 per cent completeness limits of the Subaru data at $V_0 = 23.93$ and $I_0 = 23.00$. However, the

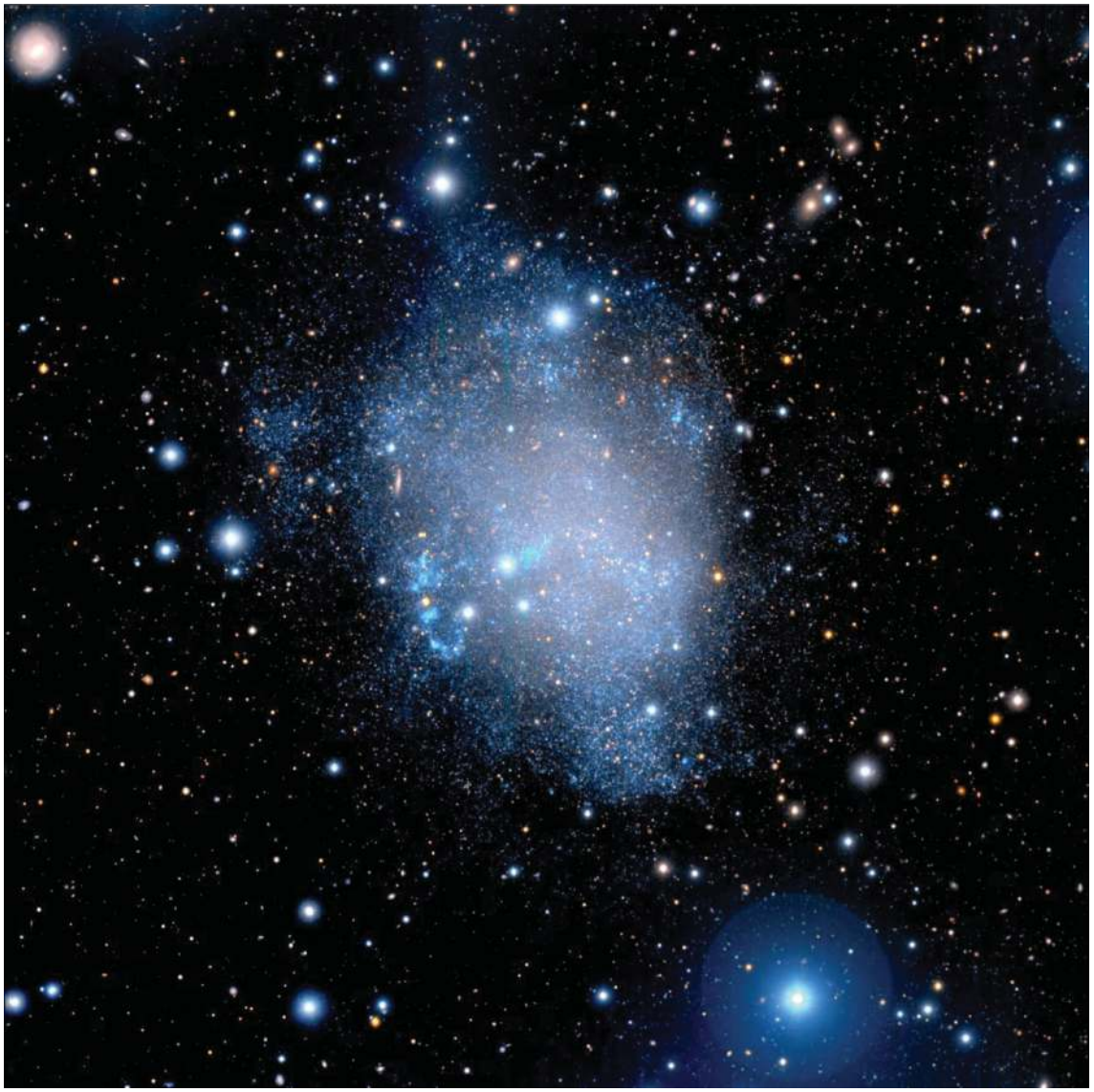

Figure 2. Colour composite mosaic of HoII from our Subaru data. The image is cropped to ∼14 arcmin on a side. North is up and east to the left.

centre of the galaxy is more affected by crowding than the outer regions, so completeness varies significantly with radius. To correct the radial density profile shown in Section 5, which uses all the stars with $I_0 < 24.5$, we therefore estimate the completeness down to this magnitude as a function of radius. The result is shown in Fig. 3. For each annulus, the error bar was calculated by adding in quadrature the Poisson uncertainties on the number of stars in the *HST* and Subaru subsamples. We find that completeness varies from 10 per cent in the inner 0.5 arcmin to 90 per cent at $R \sim 4$ arcmin. The dashed line is a fit to the points between $R = 1.5$ and 4 arcmin, and suggests that we can assume ∼100 per cent completeness beyond 4 arcmin.

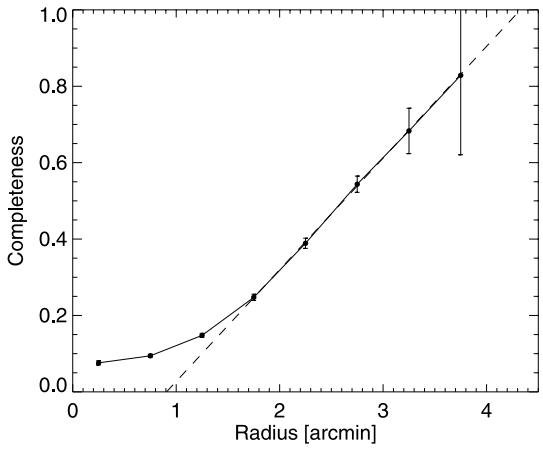

Figure 3. Completeness of the Subaru data, relative to the *HST*/ACS data, as a function of galactocentric radius for stars brighter than $I_0 = 24.5$. The dashed lines are a fit to the points between $R = 1.5$ and 4 arcmin.

3 COLOUR–MAGNITUDE DIAGRAMS

The resulting CMDs for the field and HoII stars are shown in Fig. 4. We used the 0.1 and 2×10^{20} atoms cm^{-2} H I contours to separate the two populations (see Section 4): stars outside the former are assumed to be field stars, while stars inside the latter are considered HoII stars. The CMDs were cleaned of non-stellar objects using

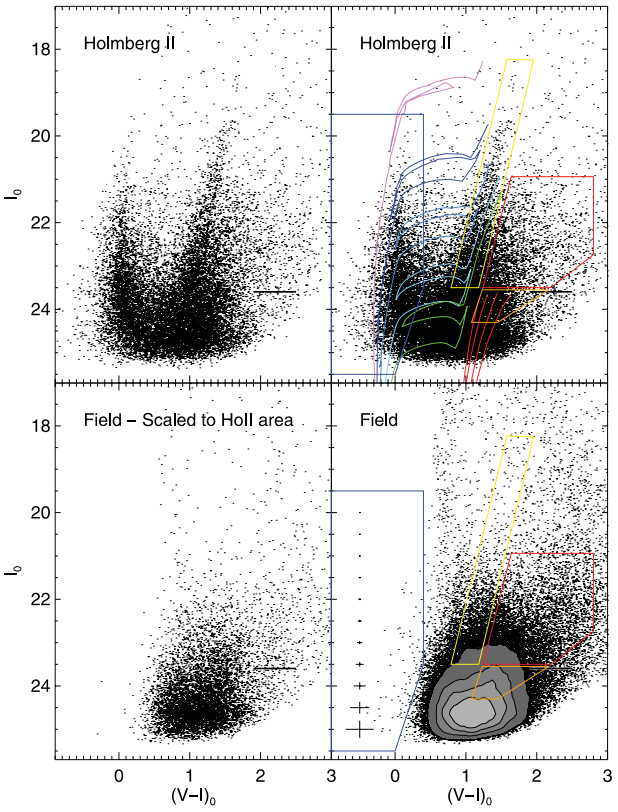

Figure 4. Extinction-corrected colour–magnitude diagrams of HoII (top panels) and field stars (bottom panels). In the bottom right-hand panel, the contour levels correspond to [6, 12, 18, 24, 30] $\times$ 10^3 stars mag^{-2}, and the error bars show the mean photometric errors as a function of magnitude for both field and HoII stars. The boxes used to select the various stellar populations are shown in the right-hand panels: MS+BSG (blue), RSG (yellow), AGB (red) and RGB (orange). Selected isochrones from the Padua library (Marigo et al. 2008) have been overplotted in the top right-hand panel (see text for details).

the photometric parameters given by ALLFRAME, namely $\sigma_{V,I} \leq 0.2$ and |SHARP| ≤ 1. To enhance the features at faint magnitudes, the CMD of the top left-hand panel was further cleaned using tighter constraints on the sharpness (|SHARP| $\leq$ 0.5) but is shown only for illustrative purpose. It contains ~16 600 stars, instead of the ~27 100 stars in the CMD of the top right-hand panel.

At I_0 brighter than ~22 the field CMD, shown in the bottom right-hand panel of Fig. 4, harbours two prominent vertical sequences: the main-sequence (MS) turn-off stars of the Milky Way (MW) halo at $(V-I)_0 \sim 0.7$ and dwarf stars in the MW disc at $(V-I)_0 \sim 2.5$. At fainter magnitudes, these sequences are overwhelmed by the contribution of unresolved background galaxies. We note, however, that the HoII CMDs in the top panels correspond to an area about 10 times smaller than that covered by the field stars, so the effect of the contamination by foreground stars and background galaxies is not as significant. To illustrate this, the bottom left-hand panel shows the CMD of a field with the same area as HoII. The scaled field CMD contains ~7600 objects.

To help identify the features in the HoII CMDs, in the top right-hand panel of Fig. 4 we overplot isochrones from the Padua stellar evolution library (Marigo et al. 2008), shifted to the distance of HoII. The young isochrones have $Z = 0.002$ and ages of 10, 20, 50, 100 and 160 Myr from the top to bottom, while the old ones shown in red are 12.5 Gyr old with $Z = 0.0001$, 0.0003, 0.001 and 0.002 from the left-hand to right-hand side.

The most prominent features of the HoII CMD are the blue and red supergiant branches (BSG and RSG branches, respectively) of core helium-burning stars at $(V-I)_0 \sim 0$ and 1.2, respectively. Their presence indicates vigorous star formation in the past ~160 Myr. The BSG branch curves towards the red below $I_0 \sim 24$, and joins the RSG close to the red clump just below our limiting magnitude. Redward of the RSG and at $I_0 \gtrsim 23.5$, a higher density of stars corresponding to the red giant branch (RGB) is visible. The expected magnitude of the tip of the RGB (TRGB), from Karachentsev et al. (2002), is shown as a thin line at $I_0 = 23.60$. Some of the stars brighter than the TRGB and redder than the RSG are genuine asymptotic giant branch (AGB) stars (see Section 4), although they are difficult to separate from the contamination of foreground stars and unresolved galaxies. Finally, a few dozen MS stars forming a diffuse band bluewards of the BSG branch are visible at about $(V-I)_0 = -0.2$ and $I_0 \gtrsim 21.5$, indicating star formation within the last 10 Myr. We note that while some of these stars lie bluewards of the youngest isochrones, their concentration close to the centre of HoII confirms that they are bona fide members of HoII. Their colour spread, larger than expected from photometric errors only, is a consequence of the crowding in this region.

In the following section, we analyse the spatial distributions of the different stellar populations individually. They are selected on the CMDs using the boxes shown in the right-hand panels of Fig. 4. The blue, yellow, red and orange boxes enclose the stars belonging to MS+BSG ($\lesssim$160 Myr), RSG (10–160 Myr), AGB (a few hundred Myr to a few Gyr) and RGB ($\gtrsim$1.5 Gyr), respectively. For the MS+BSG selection, we chose to use the whole range of luminosity since contamination by foreground and background sources is virtually non-existent in this colour range.

4 SPATIAL DISTRIBUTION

In Fig. 5 we show the spatial distribution of each individual stellar population – selected using the boxes shown in the left-hand panels of Fig. 4 – and the corresponding contours. From the top to bottom, the panels show the distribution of the MS+BSG, RSG, AGB and RGB stars. To serve as guides, in each panel we also plotted two H I contours from the BC02 study, representing densities of 0.1 and 2×10^{20} atoms cm^{-2}: the first one is their lowest density contour, while the second is the innermost contour that includes most of the observed MS+BSG stars belonging to HoII. We find that the shape of the latter contour is close to an ellipse with radius $R = 6.0$ arcmin, $b/a = 0.90$, and position angle (PA) of 27°. These are the contours we used to separate HoII from field stars (see Section 3).

The top panels show that blue stars younger than about 160 Myr old are confined to regions where the H I density is higher than about 2×10^{20} atoms cm^{-2}. Very few objects outside the contours are distributed uniformly over the FOV, suggesting that they are either unresolved galaxies with similar colours, foreground blue horizontal branch, blue straggler or white dwarf stars. The outermost MS+BSG contour follows very closely the inner H I contour, as expected, if massive star formation only occurs above a certain gas density threshold. The other panels show that contamination by field stars and unresolved galaxies increases significantly at redder colours and fainter magnitudes. Nevertheless, these maps do not show significant stellar concentrations outside the central contour, which suggests that most or all of the sources outside this area are either foreground stars or unresolved galaxies.

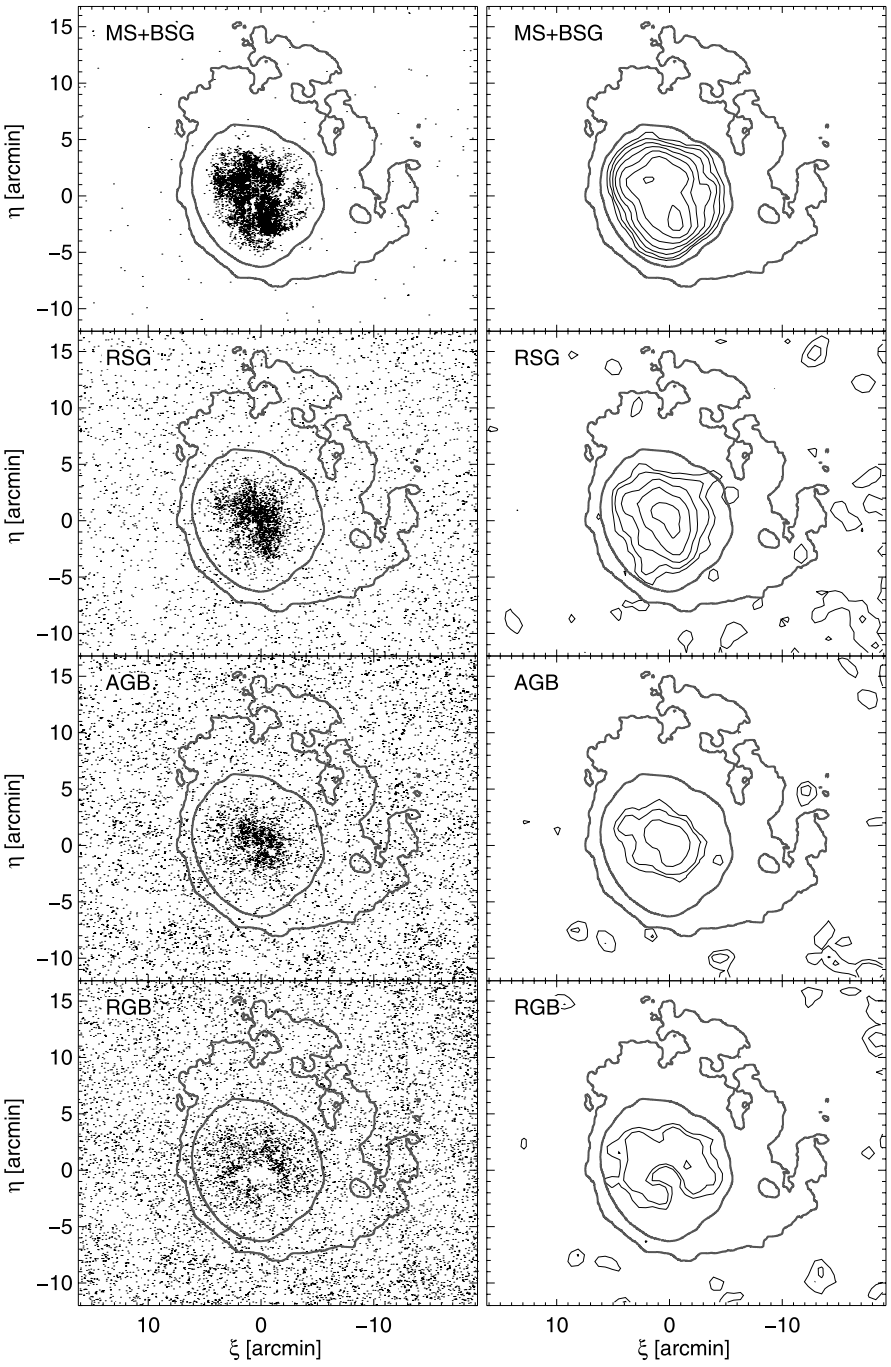

Figure 5. Spatial distribution of candidate MS+BSG, RSG, AGB and RGB stars in the whole Subaru FOV (left-hand panels) and the corresponding contours (right-hand panels). Stellar contour levels are arbitrary. The two H I contours (0.1 and 2×10^{20} atoms cm^{-2}, from BC02) used to separate HoII from field stars are shown as thick grey lines to use as guides.

Interestingly, in Fig. 5 the concentration seems to increase from BSG to RSG stars, and from RSG to AGB stars, the populations being more compact with increasing age. The RGB stars, close to our detection limit, are the most affected by crowding which explains the hole in the distribution at the centre of HoII. In addition, some of the stars flagged as RGB may actually be RSG or AGB stars that were shifted to the RGB box due to photometric errors. Therefore, since the RGB distribution is not clear from our Subaru data, we checked the distribution using the *HST*/ACS photometry of HoII described in Section 2.3. In the bottom left-hand panel of Fig. 6, we show the distribution of RGB stars in the top 1.5 mag of the RGB from the *HST* data set. The MS+BSG, RSG and AGB maps from the Subaru data are shown in the other panels. In each panel, the black line outlines the combined footprint of the two ACS pointings to facilitate comparison.

The difference between the distributions of the MS+BSG and RGB samples is striking: despite the small area covered by the *HST* data, it is obvious that the old, RGB stars are significantly more concentrated than the younger stars, as already noted by Bastian et al. (2011). The former are also distributed in a roughly circular distribution, whereas the latter present a very irregular distribution. Within the ACS footprint, the density of RGB stars almost vanishes

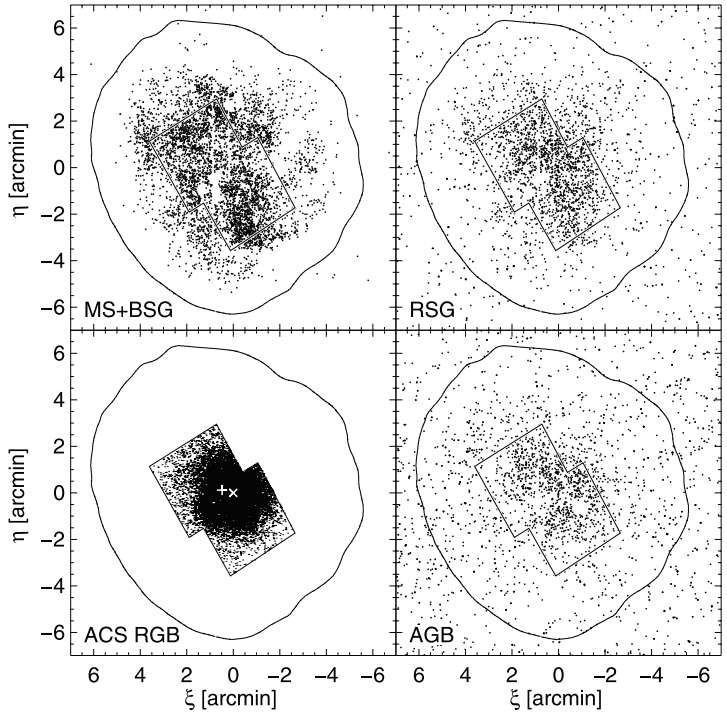

Figure 6. Zoomed-in spatial distribution of BSG, RSG and AGB stars in the Subaru FOV, and RGB stars from *HST*/ACS data. Several small holes in the stellar distributions are due to highly saturated stars and their associated bleed spikes. The inner H I contour of Fig. 5, as well as the outline of the combined footprint of the two ACS pointings, is shown. The cross and plus symbols in the bottom left-hand panel represent the dynamical centre and the centre of the H I contour, respectively, to highlight the offset between the two.

close to the edges, while the density of blue stars is roughly uniform. We note that the distributions of Subaru and *HST*/ACS blue stars are very similar in the area in common. Using only the ACS data to avoid the uncertainties due to incompleteness and different spatial coverage, we find exponential scalelengths for the MS+BSG, RSG, AGB and RGB samples of 3.1 ± 0.5, 1.7 ± 0.3, 0.80 ± 0.07 and 0.76 ± 0.04 arcmin, respectively. Given the small FOV, we did not apply a background correction to these profiles.

Fig. 6 also shows that the blue stars, besides having a larger spatial extent, also seem to delineate short spiral arms. This morphology is not due to highly saturated stars or artefacts due to image defects, and completeness down to $I_0 = 24.5$ is ∼100 per cent at large radii. These arms follow the same counterclockwise orientation as the H I arms observed by Bureau et al. (2004) in the north-west of HoII, which further suggests they are real. The lack of similar arms in the distribution of AGB stars suggests these are likely transient features.

The good agreement between the distribution of young stars and the H I gas is further illustrated in Fig. 7. The left-hand panel presents the distribution of MS+BSG stars overlaid on the H I contours of BC02, and shows that these are usually located in the higher column density areas. In the right-hand panel, we plot the number of MS+BSG stars in bins of 37.5 arcsec on a side as a function of the H I density in the same bins. Note that for this panel we have used the higher resolution map of Walter et al. (2008, natural weighting, beam size ∼13 arcsec) to better sample the scales of our stellar distribution. It shows that the distributions of young stars and H I gas are correlated. A few points at high gas density and low star counts are artefacts due to the holes left by very saturated stars and their bleed spikes. On the other hand, the data points with high stellar and low gas density are real: most of them are located in the main H I hole at $\xi \sim 0$ arcmin and $\eta \sim -2$ arcmin, where Weisz et al. (2009) found elevated star formation about 50 Myr ago, but only low levels in the past 10–20 Myr. Interestingly, even though we use the number of MS+BSG stars (i.e. younger than about 150 Myr) as a rough proxy for the star formation rate (SFR), we find that the line representing the typical Kennicutt–Schmidt relation with a slope of 1.4 (Kennicutt 1998) provides a good match to our data.

Another interesting characteristic in Fig. 6 is the apparent offset between the centres of the MS+BSG and *HST*/RGB star distributions, shown in the bottom left-hand panel as the open circle and cross, respectively. We note that we applied a small shift ($\lesssim$4 arcsec) to the astrometry of the *HST* data to correct for a slight mismatch between the two catalogues, so the offset is not due to inaccurate astrometry. We find that the dynamical centre listed in Stewart et al. (2000, $\alpha_{2000} = 8^{\rm h}19^{\rm m}05\overset{\rm s}{.}6$, $\delta_{2000} = 70^{\circ}43'25''$) provides an excellent fit to the distribution of RGB stars. On the other hand, the centre of the inner H I contour, which follows very closely the distribution of MS+BSG stars, is offset from the dynamical centre by 30 arcsec (0.49 kpc) east and 7 arcsec (0.1 kpc) north. While the origin of this shift is unclear, it is reasonable to suspect that it is related to the processes that shaped the outer H I envelope.

5 RADIAL PROFILE

In order to obtain the radial density profile of HoII, one needs a reliable estimate of its ellipticity, PA and the location of its centre. We use the dynamical centre described in the previous section, which is also the centre of the intermediate-age and old stellar populations ($\gtrsim$1.5 Gyr old). The large uncertainty on the inclination of HoII (BC02; de Blok et al. 2008; Walter et al. 2008; Oh et al. 2011; Gentile et al. 2012) prevents us from properly constraining the morphology of the galaxy. However, given the very low ellipticity of the inner H I contours ($1 - b/a \sim 0.1$) and circular distribution

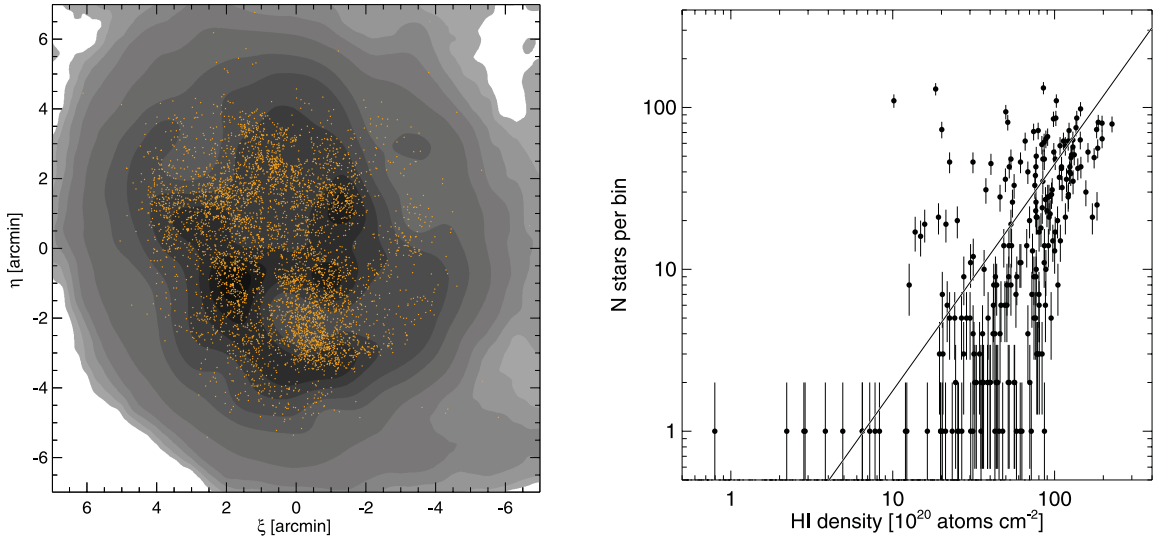

Figure 7. Left-hand panel: spatial distribution of MS+BSG stars overlaid on the H I contours of BC02. Right-hand panel: surface density of MS+BSG stars as a function of H I density in square bins of 37.5 arcsec a side. The solid line represents the typical Kennicutt–Schmidt relation with a slope of 1.4 (Kennicutt 1998).

of the RGB stars, we can assume circular symmetry for the purpose of calculating the radial profiles.

While resolved star counts are the optimal way to probe the very low surface brightness structure of galaxies (e.g. Barker et al. 2009), they are not ideal at small radii due to crowding and incompleteness. As described in Section 2.3, crowding is particularly severe in the central part of HoII. However, it is possible to use diffuse light in this area and combine the contribution of both to obtain a composite profile extending over the whole radius.

For the diffuse light surface brightness profile, we used the median pixel value in concentric circles, after masking the saturated stars and their associated bleed spikes, as well as bright background galaxies. The sky value was estimated from the mode of the pixel value distribution of the entire image. The pixel values were then converted to mag arcsec^{-2}, calibrated using the same zero-point as for the stellar photometry, and corrected for reddening using $E(B-V) = 0.032$ (Schlegel et al. 1998).

The same concentric circles were used for the star count profile, in which we counted the number of stars brighter than $I_0 = 24.5$. This limit was chosen as the best compromise between sufficient number statistics and reasonable completeness correction. The background contaminant level was estimated from the density of point sources in a wide circular annulus in a region where HoII's radial profile is flat within the uncertainties ($7.5 \leq r \leq 10.5$ arcmin). For the area covered by the *HST* data, we applied the correction for completeness determined in Section 2.3. As for the diffuse light, the radial density profile $\Sigma(r)$ was then converted to a magnitude scale using the relation $\mu(r) = -2.5\log \Sigma(r) + \mathrm{ZP}$. However, here the zero-point ZP was estimated by matching the overlapping region of the stellar and diffuse light profiles ($2.5 \lesssim r \lesssim 4$ arcmin).

The resulting profiles are presented in Fig. 8: the diffuse light and stellar surface brightness profiles are shown as the grey filled circles and black filled stars, respectively. The open stars show the completeness-corrected star count profile. Although the completeness-corrected star counts and the diffuse light give reassuringly similar information in the inner regions, the star count data allow the profile to be extended to $R \sim 7$ arcmin where $\mu_V \sim 32$ mag arcsec^{-2}.

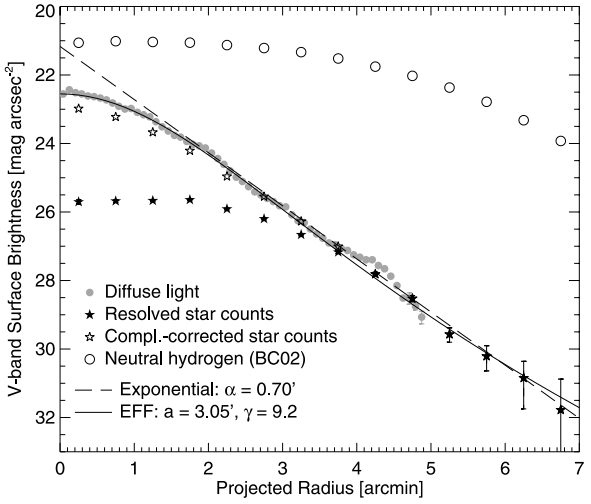

Figure 8. Background-subtracted surface brightness profiles from the diffuse light (grey filled circles), resolved star counts (filled stars) and completeness-corrected star counts (open stars). The open circles represent the H I density profile, from BC02. The dashed and solid lines are exponential and EFF profiles fitted to the composite surface brightness profile (see text).

The surface brightness is well described by an inner core (to ∼1.5 arcmin) and a smooth outer decline. We find that an EFF (Elson, Fall & Freeman 1987) profile provides the best description over the entire radial range, while an exponential fit also works beyond the inner core. On the other hand, the King (1962) and Plummer (1911) profiles (not shown) tend to under- and over-estimate the stellar density beyond ∼3 arcmin, respectively. The exponential fit to the profile between $R = 1.5$ and 7 arcmin is shown as the dashed line, and has a scalelength of 0.70 ± 0.01 arcmin, or 0.69 ± 0.01 kpc at the distance of HoII. The EFF fit (solid line) leads to a half-light radius of 1.41 ± 0.04 arcmin (i.e. 1.39 ± 0.04 kpc) and absolute magnitude $M_V = -16.3$.

Our scalelength is slightly smaller than the estimates from Swaters (1999, $h_B = 0.99$ arcmin and $h_R = 0.86$ arcmin after correcting for the difference in ellipticity). The discrepancy between the two estimates is most likely due to a combination of the shallower depth of their data ($\mu_R \lesssim 27.5$) and the steepening of our profile at larger radii. On the other hand, the radial profile of HoII shown in Oh et al. (2011) extends farther out than the one presented here (out to $R \sim 9$ kpc). We believe their extent may be overestimated as a consequence of using a relatively large ellipticity ($b/a \sim 0.66$), and a PA determined from the H I data (175°) which is offset by about 35° from the PA of the optical data (30°; Swaters 1999).

We thus find that the stellar component of HoII is significantly more compact than the H I cloud in which it is embedded, which extends out to ∼16 arcmin (BC02). Even if some stars belonging to HoII are present beyond $R \sim 7$ arcmin, their contribution to the galaxy luminosity is likely to be negligible. Assuming an exponential profile, such a population would represent less than 0.1 per cent of the total galaxy light.

6 DISCUSSION

6.1 Global structure

Using the resolved stars counts in the outer regions of HoII revealed an extended structure that is an order of magnitude fainter than what can be reached with diffuse light. Outside the central 2 arcmin area, the profile is well fitted by an exponential model out to $R = 7$ arcmin with a scalelength of 0.69 ± 0.01 kpc. However, we have also found that the scalelength is different for each stellar population, in the sense that it decreases with increasing age. This is contrary to what is usually observed in dwarf galaxies in the nearby Universe (e.g. Zhang et al. 2012), where the region of active star formation has been shrinking with time. This implies that HoII would have been a more compact galaxy in the past. The very low density of RGB stars in the outskirts of the *HST* fields compared to that of the younger stars can be interpreted as a significantly lower SFR in these parts $\gtrsim$1.5 Gyr ago (the minimum age of stars in the top magnitude of the RGB) than in the past ∼160 Myr. This is in good agreement with the star formation histories (SFHs) obtained from these *HST* data, which show a higher SFR starting about 300 Myr ago (Dalcanton et al. 2012, see also McQuinn et al. 2010), as well as a 'dramatic rise in the SFR over the past 50 Myr' (Weisz et al. 2008).

Given the large amount and relatively high density of the neutral hydrogen surrounding HoII (BC02), it is somewhat surprising that star formation was not more vigorous prior to about 300 Myr. This could suggest that the extended H I has recently been acquired or that it previously had too low a density for star formation to be significant. The process that shaped the spectacular H I envelope could have also increased the gas pressure in the inner regions of the galaxy and triggered the large-scale star formation that we observe today. Two potential mechanisms to explain this are ram pressure by a hot IGM and a tidal interaction with a companion galaxy, which we discuss and compare below.

6.2 Origin of the H I morphology

HoII is embedded in a massive H I cloud that is significantly more extended than the optical counterpart. The remarkable morphology of the cloud in the low-density outskirts, compressed on one side with a cometary appearance on the opposite side (see Fig. 1), is very suggestive of ram pressure stripping due to the presence of a hot IGM. While there are no X-ray observations to date confirming the presence of diffuse hot gas in the vicinity of HoII, such observations are available for other much smaller, 'poor' groups (e.g. Zabludoff & Mulchaey 1998) in which the hot IGM density can be as high as $\sim 5 \times 10^{-4}$ atoms cm^{-3} (Mulchaey et al. 1993; Sun 2012), that is, about two orders of magnitude higher than the minimum IGM density necessary to strip the interstellar medium (ISM) of a low-mass dwarf galaxy like HoII (e.g. BC02, McConnachie et al. 2007).

However, the disturbed appearance of the gas cloud may also be the result of gravitational interactions. While HoII is relatively isolated from the massive galaxies of the M81 group (see Fig. 9), it has at least two companion dwarf galaxies within a projected distance of ∼100 kpc which may have tidally affected the neutral hydrogen cloud. BC02 discussed the possible origins of the H I morphology and concluded that the ram pressure and tidal interaction scenarios were both plausible, given the available information. Their follow-up study, despite the significant improvement in both coverage and sensitivity, was not sufficient to rule out one or the other scenario (Bureau et al. 2004). They suggested that deep stellar photometry could resolve the issue by revealing a stellar counterpart to the north-west H I structure, since ram pressure is not expected to have an effect on stars. Here we summarize the current arguments in favour of each scenario and discuss whether our deep photometry may help elucidate which is the main mechanism at play.

The deeper H I observations of Bureau et al. (2004) revealed that the low surface brightness component in the north-west of HoII can be resolved in two or three arms, which are often associated with tidal interaction events (e.g. Dobbs et al. 2010). As shown in Section 4, the MS+BSG star distribution appears slightly distorted too, with spiral arm-like features south and west of HoII. The stellar arms also follow the same counterclockwise orientation as the H I arms. However, Bureau et al. (2004) also noted that the arm kinematics followed the regular rotation of the inner gas, contrary to what would be expected if they were torn from the main body by tidal interactions. In addition, while the young stars do seem to trace spiral arms, the older populations have a much more regular circular distribution. Tidal forces would affect all populations equally and the resulting stellar arms and/or tails would be made of stars of all ages. This suggests that most of the recent star formation occurred in the denser H I arms, resulting in a similar arm-like distribution of the young stars, rather than stellar tails due to tidal forces. The H I arms, in turn, could be the consequence of ram pressure, as models that include gas cooling have shown that it can produce spiral arms (e.g. Schulz & Struck 2001; Vollmer 2003; Mapelli, Moore & Bland-Hawthorn 2008).

Further insight comes from the detailed SFHs of HoII by Weisz et al. (2008) and Dalcanton et al. (2012), which reveal a significant enhancement in the last few hundred million years. Could this enhancement also be a consequence of the process that led to the striking morphology of the H I cloud? Strong bursts of star formation are often caused by an external trigger such as an accretion event or interaction with a nearby galaxy (e.g. Kennicutt et al. 1987; Bernard et al. 2012; Cignoni et al. 2012). Indeed, as shown in Fig. 9, HoII has two close companion dwarf galaxies: M81dwA (= Kar52) located at a projected distance of ∼30 kpc to the north-east and UGC 4483, ∼110 kpc to the south-east. The former, in particular, is sufficiently close that the time-scale of a past interaction is roughly compatible with the enhanced SFR found by Dalcanton et al. (2012). Assuming a relative velocity of 100 km s^{-1} (the difference of radial velocities is ∼45 km s^{-1}; Karachentsev et al. 2002) means that M81dwA could have passed close to HoII about 300 Myr ago, in good agreement with the beginning of the SFR enhancement. Both companion dwarfs also appear to have been experiencing higher star formation

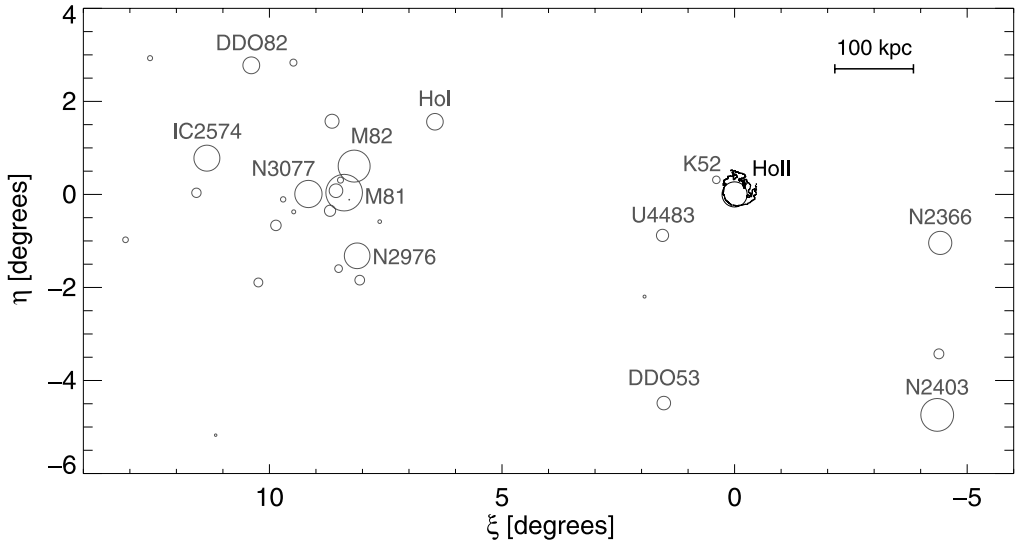

Figure 9. Distribution of galaxies in the M81 group in standard coordinates, where the symbol size is proportional to the apparent integrated *B*-band magnitude (Karachentsev et al. 2002). HoII is shown as the black circle at (0,0), and the main galaxies of the group are labelled. The outermost H I contour of HoII from BC02 is also shown, scaled up in size by a factor of 2.

in the past few hundred million years than at older epochs (McQuinn et al. 2010; Warren et al. 2011).

However, tidal interaction is not the only process that can lead to enhanced star formation. In fact, hydrodynamical and *N*-body simulations of the interaction between the hot IGM and the ISM of a galaxy have shown that ram pressure can also result in increased star formation in the inner regions. The shock waves resulting from the gas collision can increase significantly the central gas surface density and lead to the collapse of molecular clouds, thus enhancing the SFR (Quilis, Moore & Bower 2000; Schulz & Struck 2001; Vollmer et al. 2001; Marcolini, Brighenti & D'Ercole 2003). The fact that the spatial distribution of young stars closely follows that of the H I contours strongly supports this interpretation. Such an enhancement of the star formation as a consequence of the interaction between ISM and IGM has also been observed in various galaxies as asymmetric Hα enhancements, usually located along the leading edge of the galaxy disc (e.g. Koopmann & Kenney 2004; Crowl et al. 2005).

Therefore, while the morphology of the H I cloud and the observed enhancement of the recent SFR cannot help discriminate between the phenomena at play, the regular circular distribution of the intermediate-age and old stars, the regular rotation of the H I arms, the undisturbed H I distribution of the two nearest dwarf companions and the lack of H I bridges/filaments between them and HoII (Bureau et al. 2004; Chynoweth et al. 2009; Ott et al. 2012), all support the ram pressure stripping scenario. In addition, we do not find a stellar counterpart to the H I cloud beyond $R \sim 7$ arcmin where it becomes distorted and forms arms/tails, whereas tidal forces would affect gas and stars equally. Therefore, our data strongly suggest that ram pressure stripping is the main process responsible for the swept-back appearance of the H I cloud.

7 SUMMARY AND CONCLUSIONS

We have carried out a wide-field survey of the M81 group dwarf galaxy HoII based on deep Subaru/Suprime-Cam imaging in *V* and *I*. These observations cover the whole extent of the galaxy, including the vast H I cloud, and allow us to perform photometry of individual stars down to $I \sim 25.2$, that is, about 1.5 mag below the tip of the RGB.

The deep CMDs reveal the presence of stellar populations of all ages, from a few Myr old (MS+BSG, RSG) to several Gyr old (RGB). While in most dwarf galaxies in the local Universe the younger stars are found to be more centrally concentrated than the older populations (e.g. Zhang et al. 2012), we find that in HoII the old RGB stars are significantly more concentrated than the young MS+BSG stars. Indeed, we find that the exponential scalelength for the young MS+BSG population is much larger than that of the RGB component (2.8 ± 0.4 arcmin versus 0.76 ± 0.04 arcmin, respectively). We speculate that the shock wave due to ram pressure increased the gas density in the central part of the H I cloud and triggered star formation on large scales.

Our Subaru data enable us to construct a composite surface brightness profile for HoII by combining diffuse light in the central region with star counts at large radii. This profile is one of the deepest yet published for any galaxy, extending from the centre out to $R \sim 7$ arcmin where $\mu_V = 32$ mag arcsec^{-2}. Fitting an exponential profile to the outer regions gives a (projected) scalelength of 0.70 ± 0.01 arcmin, corresponding to 0.69 ± 0.01 kpc at the distance of HoII.

Finally, we discuss the properties of the resolved stellar populations in the context of the morphology of the large H I cloud in order to understand the origin of its swept-back, cometary appearance. Previous studies based on diffuse optical light or 21-cm data could not definitively determine whether the cloud shape was due to ram pressure from a hot IGM or due to a tidal interaction with a nearby companion galaxy. Our deep photometry shows that the intermediate-age and old stars have a regular circular distribution and show no sign of tidal tails/streams. In addition, we find that there are very few, if any, HoII stars beyond $R \sim 7$ arcmin where the H I becomes distorted. Since tidal forces would affect gas and stars equally, our data strongly suggest that the spectacular morphology of the H I cloud is due to ram pressure. The detection of a significant amount of diffuse hot gas in the vicinity of HoII would further verify this.

ACKNOWLEDGMENTS

We are very grateful to the anonymous referee for a prompt report that helped us improve the manuscript, and would like to thank M. Bureau for providing the H I density map of HoII. Support for this work was provided by a rolling grant from the Science and Technology Facilities Council. We acknowledge the usage of the HyperLeda data base (http://leda.univ-lyon1.fr). This research has made use of THINGS, 'The H I Nearby Galaxy Survey' (Walter et al. 2008), and the NASA/IPAC Infrared Science Archive, which is operated by the Jet Propulsion Laboratory, California Institute of Technology, under contract with the National Aeronautics and Space Administration.

REFERENCES

Barker M. K., Ferguson A. M. N., Irwin M., Arimoto N., Jablonka P., 2009, AJ, 138, 1469
Barker M. K., Ferguson A. M. N., Irwin M. J., Arimoto N., Jablonka P., 2012, MNRAS, 419, 1489
Bastian N. et al., 2011, MNRAS, 412, 1539
Bernard E. J. et al., 2012, MNRAS, 420, 2625
Bureau M., Carignan C., 2002, AJ, 123, 1316 (BC02)
Bureau M., Walter F., van Gorkom J., Carignan C., 2004, in Duc P.-A., Braine J., Brinks E., eds, Proc. IAU Symp. 217, Recycling Intergalactic and Interstellar Matter. Astron. Soc. Pac., San Francisco, p. 452
Chung A., van Gorkom J. H., Kenney J. D. P., Vollmer B., 2007, ApJ, 659, L115
Chynoweth K. M., Langston G. I., Holley-Bockelmann K., Lockman F. J., 2009, AJ, 138, 287
Cignoni M., Cole A. A., Tosi M., Gallagher J. S., Sabbi E., Anderson J., Grebel E. K., Nota A., 2012, ApJ, 754, 130
Coleman M. G., Da Costa G. S., Bland-Hawthorn J., Freeman K. C., 2005, AJ, 129, 1443
Condon J. J., 1983, ApJS, 53, 459
Crowl H. H., Kenney J. D. P., van Gorkom J. H., Vollmer B., 2005, AJ, 130, 65
Cutri R. M. et al., 2003, The IRSA 2MASS All-Sky Point Source Catalog. NASA/IPAC Infrared Science Archive (http://irsa.ipac.caltech.edu/applications/Gator)
Dalcanton J. J. et al., 2009, ApJS, 183, 67
Dalcanton J. J. et al., 2012, ApJS, 198, 6
de Blok W. J. G., Walter F., 2006, AJ, 131, 343
de Blok W. J. G., Walter F., Brinks E., Trachternach C., Oh S.-H., Kennicutt R. C., Jr, 2008, AJ, 136, 2648
Dobbs C. L., Theis C., Pringle J. E., Bate M. R., 2010, MNRAS, 403, 625
Elson R. A. W., Fall S. M., Freeman K. C., 1987, ApJ, 323, 54
Gavazzi G., Contursi A., Carrasco L., Boselli A., Kennicutt R., Scodeggio M., Jaffe W., 1995, A&A, 304, 325
Gentile G., Angus G. W., Famaey B., Oh S.-H., de Blok W. J. G., 2012, A&A, 543, A47
Greisen E. W., Calabretta M. R., 2002, A&A, 395, 1061
Hidalgo S. L., Aparicio A., Martínez-Delgado D., Gallart C., 2009, ApJ, 705, 704
Holmberg E., 1950, Lund Medd. Astron. Obs. Ser. II, 128, 1
Irwin M. J., 1985, MNRAS, 214, 575
Irwin M. J., 1997, in Rodriguez Espinosa J. M., Herrero A., Sánchez F., eds, Instrumentation for Large Telescopes. Cambridge Univ. Press, Cambridge, p. 35
Irwin M., Lewis J., 2001, New Astron. Res., 45, 105
Irwin M. J. et al., 2004, in Quinn P. J., Bridger A., eds, Proc. SPIE Vol. 5493, Optimizing Scientific Return for Astronomy through Information Technologies. SPIE, Bellingham, p. 411
Karachentsev I. D. et al., 2002, A&A, 383, 125
Kenney J. D. P., van Gorkom J. H., Vollmer B., 2004, AJ, 127, 3361
Kennicutt R. C., Jr, 1998, ApJ, 498, 541
Kennicutt R. C., Jr, Roettiger K. A., Keel W. C., van der Hulst J. M., Hummel E., 1987, AJ, 93, 1011
King I., 1962, AJ, 67, 471
Koopmann R. A., Kenney J. D. P., 2004, ApJ, 613, 866
Lasker B. M. et al., 2008, AJ, 136, 735
McConnachie A. W., Irwin M. J., Ibata R. A., Ferguson A. M. N., Lewis G. F., Tanvir N., 2003, MNRAS, 343, 1335
McConnachie A. W., Venn K. A., Irwin M. J., Young L. M., Geehan J. J., 2007, ApJ, 671, L33
McQuinn K. B. W. et al., 2010, ApJ, 724, 49
Mapelli M., Moore B., Bland-Hawthorn J., 2008, MNRAS, 388, 697
Marcolini A., Brighenti F., D'Ercole A., 2003, MNRAS, 345, 1329
Marigo P., Girardi L., Bressan A., Groenewegen M. A. T., Silva L., Granato G. L., 2008, A&A, 482, 883
Miyazaki S. et al., 2002, PASJ, 54, 833
Mulchaey J. S., Davis D. S., Mushotzky R. F., Burstein D., 1993, ApJ, 404, L9
Oh S.-H., de Blok W. J. G., Brinks E., Walter F., Kennicutt R. C., Jr, 2011, AJ, 141, 193
Ott J. et al., 2012, AJ, 144, 123
Paturel G., Petit C., Prugniel P., Theureau G., Rousseau J., Brouty M., Dubois P., Cambrésy L., 2003, A&A, 412, 45
Plummer H. C., 1911, MNRAS, 71, 460
Quilis V., Moore B., Bower R., 2000, Sci, 288, 1617
Ryder S. D., Purcell G., Davis D., Andersen V., 1997, PASA, 14, 81
Ryś A., Grocholski A. J., van der Marel R. P., Aloisi A., Annibali F., 2011, A&A, 530, A23
Schlegel D. J., Finkbeiner D. P., Davis M., 1998, ApJ, 500, 525
Schulz S., Struck C., 2001, MNRAS, 328, 185
Stanimirovic S., Staveley-Smith L., Dickey J. M., Sault R. J., Snowden S. L., 1999, MNRAS, 302, 417
Stanimirović S., Staveley-Smith L., Jones P. A., 2004, ApJ, 604, 176
Stetson P. B., 1993, in Butler C. J., Elliott I., eds, Proc. IAU Symp. 136, Stellar Photometry – Current Techniques and Future Developments. Cambridge Univ. Press, Cambridge, p. 291
Stetson P. B., 1994, PASP, 106, 250
Stewart S. G. et al., 2000, ApJ, 529, 201
Stinson G. S., Dalcanton J. J., Quinn T., Gogarten S. M., Kaufmann T., Wadsley J., 2009, MNRAS, 395, 1455
Sun M., 2012, New J. Phys., 14, 045004
Swaters R. A., 1999, PhD thesis, Rijksuniversiteit Groningen, http://irs.ub.rug.nl/ppn/186373880
Vollmer B., 2003, A&A, 398, 525
Vollmer B., Cayatte V., Balkowski C., Duschl W. J., 2001, ApJ, 561, 708
Walter F. et al., 2007, ApJ, 661, 102
Walter F., Brinks E., de Blok W. J. G., Bigiel F., Kennicutt R. C., Jr, Thornley M. D., Leroy A., 2008, AJ, 136, 2563
Warren S. R. et al., 2011, ApJ, 738, 10
Weisz D. R., Skillman E. D., Cannon J. M., Dolphin A. E., Kennicutt R. C., Jr, Lee J., Walter F., 2008, ApJ, 689, 160
Weisz D. R., Skillman E. D., Cannon J. M., Dolphin A. E., Kennicutt R. C., Jr, Lee J., Walter F., 2009, ApJ, 704, 1538
Weisz D. R. et al., 2011, ApJ, 739, 5
Westfall K. B., Majewski S. R., Ostheimer J. C., Frinchaboy P. M., Kunkel W. E., Patterson R. J., Link R., 2006, AJ, 131, 375
Zabludoff A. I., Mulchaey J. S., 1998, ApJ, 496, 39
Zhang H.-X., Hunter D. A., Elmegreen B. G., Gao Y., Schruba A., 2012, AJ, 143, 47

This paper has been typeset from a TEX/LATEX file prepared by the author.